Inorganic Chemistry

Article

pubs.acs.org/IC

Cation Substitution Dependent Bimodal Photoluminescence in Whitlockite Structural $Ca_{3-x}Sr_x(PO_4)_2:Eu^{2+}$ ($0 \le x \le 2$) Solid Solution Phosphors

Haipeng Ji,[†] Zhaohui Huang,*[,†] Zhiguo Xia,*[,‡] Maxim S. Molokeev,[§] Victor V. Atuchin,[∥,⊥,#] and Saifang Huang[†,▽]

[†]School of Materials Science and Technology, China University of Geosciences (Beijing), Beijing 100083, People's Republic of China

[‡]School of Materials Sciences and Engineering, University of Science and Technology Beijing, Beijing 100083, People's Republic of China

[§]Laboratory of Crystal Physics, Kirensky Institute of Physics, SB RAS, Krasnoyarsk 660036, Russia

[∥]Laboratory of Optical Materials and Structures, Institute of Semiconductor Physics, SB RAS, Novosibirsk 630090, Russia

[⊥]Functional Electronics Laboratory, Tomsk State University, Tomsk 634050, Russia

[#]Laboratory of Semiconductor and Dielectric Materials, Novosibirsk State University, Novosibirsk 630090, Russia

[▽]Department of Chemical and Materials Engineering, The University of Auckland, PB 92019, Auckland 1142, New Zealand

Supporting Information

ABSTRACT: Cation substitution dependent tunable bimodal photoluminescence behavior was observed in the $Ca_{3-x}Sr_x(PO_4)_2:Eu^{2+}$ ($0 \le x \le 2$) solid solution phosphors. The Rietveld refinements verified the phase purity and whitlockite type crystal structure of the solid solutions. The tunable photoluminescence evolution was studied as a function of strontium content, over the composition range $0.1 \le x \le 2$. In addition to the emission band peak at 416 nm in $Ca_3(PO_4)_2:Eu^{2+}$, the substitution of Ca^{2+} by Sr^{2+} induced the emerging broad-band peak at 493−532 nm. A dramatic red shift of the emission peak located in the green-yellow region was observed on an increase of x in the samples with $0.75 \le x \le 2.00$. The two emission bands could be related to the EuO_n−Ca_9 and EuO_n−$Ca_{9-x}Sr_x$ emitting blocks, respectively. The values for the two kinds of emitting blocks in the solid solutions can be fitted well with the observed intensity evolution of the two emission peaks.

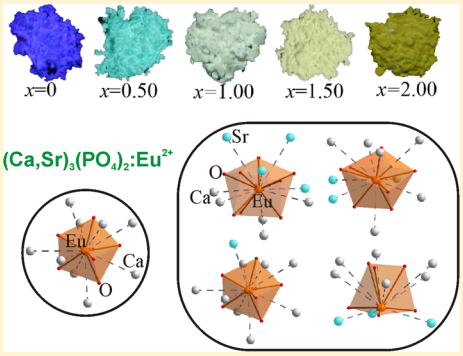

1. INTRODUCTION

Phosphor materials play a key role in the fabrication of phosphor-converted white light emitting diode (w-LED) devices based on the InGaN chip.[1,2] Recently, phosphate compounds were emerging as an important phosphor host family due to their relatively low sintering temperature, good thermal stability, and tetrahedral rigid three-dimensional matrix which is optimal for charge stabilization.[3] In recent years, intense attention has been paid to rare earth activated phosphates such as $ABPO_4$ (where A is the monovalent cation and B is the divalent cation),[4,5] $Ca_9M(PO_4)_7$ (M = Gd, La, Lu, Y),[6−9] $M_3Ln(PO_4)_3$, (Ln = Lu, Gd, Sc, Tb, Y; M = Ba, Sr),[10−15] $KCaY(PO_4)_2$,[16] $Ca_{10}K(PO_4)_7$,[17] and $Sr_8MgLn(PO_4)_7$ (Ln = Y, La).[18] Dominantly, the compounds possess a crystal structure similar to that of β-$Ca_3(PO_4)_2$[19] or natural mineral whitlockite, $Ca_{18.19}(Mg_{1.17}Fe_{0.83})H_{1.62}(PO_4)_{14}$.[20]

β-$Ca_3(PO_4)_2$ can be regarded as synthetic whitlockite. The β-$Ca_3(PO_4)_2$ structure permits heterovalent substitution of Ca^{2+} by univalent metals M^+ with the formula $MCa_{10}(PO_4)_7$ (M = Li, Na, K, Cs, Ag),[21,22] by trivalent metals R^{3+} with the formula $Ca_9R(PO_4)_7$ (R = Cr, Fe, Ln),[23,24] or by combinations of univalent and trivalent metals,[25] yielding a large number of synthetic whitlockite family compounds.[26,27] These new phases reasonably preserve a polar whitlockite-type structure and have served as the basis for the crystallochemical design to achieve pronounced catalytic, ferroelectric, nonlinear optical, and ion conductive properties.[28,29] Due to the interesting crystal chemistry and adjustable crystal field environment, whitlockite-related structures acting as phosphor hosts have attracted growing interest.[30]

This study of the whitlockite structural phosphors is focused on the Ca↔Sr cation substitution effects in the β-$Ca_3(PO_4)_2:Eu^{2+}$ framework, where unusual cation substitution dependent photoluminescence evolution has been achieved in $Ca_{3-x}Sr_x(PO_4)_2:Eu^{2+}$ solid solutions. Previously, we reported a new phosphor with the composition $Sr_{1.75}Ca_{1.25}(PO_4)_2:Eu^{2+}$ as a yellow component for application in a near-ultraviolet (UV) light pumped w-LED, and the crystal structure was well refined using the whitlockite parameters.[31] Under UV light irradiation,

Received: July 16, 2014
Published: September 30, 2014

   dx.doi.org/10.1021/ic501679f | Inorg. Chem. 2014, 53, 11119−11124

the $Ca_3(PO_4)_2$:Eu^{2+} phosphor emits blue light, while the Sr^{2+} doping of $Ca_3(PO_4)_2$:Eu^{2+} induces tunable green or yellow light emission. However, several crucial issues concerning the structural evolution of these solid solutions on doping and the composition ranges remain unclear, such as the strong red shift in luminescence. In addition, very interestingly, cation substitution dependent bimodal band photoluminescence was observed in these solid solution phosphors. In the present study, the tunable photoluminescence of $Ca_{3-x}Sr_x(PO_4)_2$:Eu^{2+} (x = 0−2) was evaluated over the range x = 0.10−2.00, and the structural alteration was characterized by Rietveld refinements. An interesting model is proposed to interpret the photoluminescence evolution and structure−property relationship, which would be very important for the further study of the inorganic phosphor materials.

2. EXPERIMENTAL SECTION

2.1. Materials and Synthesis. The $Ca_{3-x}Sr_x(PO_4)_2$:$0.04Eu^{2+}$ ($0 \le x \le 2$) solid solutions were synthesized by a high-temperature solid-state reaction starting from $SrCO_3$ (A.R.), $CaCO_3$ (A.R.), $NH_4H_2PO_4$ (A.R.), and Eu_2O_3 (99.99%) (Beijing Chemical Company, Beijing, People's Republic of China). After they were weighed and thoroughly mixed, the stoichiometric raw material mixtures were placed into corundum crucibles, preheated at 700 °C for 3 h in a muff furnace in the air to release the NH_3, CO_2, and H_2O components, and finally sintered at 1250 °C for 7 h in a tube furnace under the reducing 5% H_2−95% N_2 gas flow. After that, the samples were furnace-cooled to room temperature and ground into powder for further characterization.

2.2. Characterization. The powder X-ray diffraction (XRD) patterns of the phosphors were recorded by an X-ray diffractometer (D/max-IIIA, Rigaku Corporation, Japan) operated at 40 kV and 100 mA, using Cu Kα radiation (1.5406 Å). The step scanning rate selected for detailed spectra was 2 s/step with a step size of 0.02°, and the curves were used for Rietveld analysis. The diffraction patterns were analyzed with the profile refinement program TOPAS 4.2.[32] The photoluminescence emission (PL) and excitation (PLE) spectra were measured at room temperature on a fluorescence spectrophotometer (F-4600, Hitachi, Japan) with a photomultiplier tube operating at 400 V, and a 150 W Xe lamp was used as the excitation lamp.

3. RESULTS AND DISCUSSION

Two polymorphic modifications are known for the $Sr_3(PO_4)_2$ phosphate: i.e., the α and β types. The low-temperature α form possessing a rhombohedral structure (space group $R\bar{3}m$) undergoes a polymorphic transition to the high-temperature β form (space group $R3c$) at ∼1305 °C. The transformation is reversible, and the β form cannot be overcooled to room temperature even by quenching.[33] As for the three polymorph types of $Ca_3(PO_4)_2$ denoted α, α', and β, the high-temperature forms α and α' are stable above 1430 and 1135−1430 °C, respectively, and the room temperature stable β-$Ca_3(PO_4)_2$ crystallizes in the noncentrosymmetric polar space group $R3c$.[34] The wide range of cation substitution of Ca by Sr in β-$Ca_3(PO_4)_2$ can be considered as a promising method for the solid solution preparation in the quasi-binary set $Ca_3(PO_4)_2$−$Sr_3(PO_4)_2$. However, due to the structural inconsistency between the room temperature stable β-$Ca_3(PO_4)_2$ ($R3c$) and α-$Sr_3(PO_4)_2$ ($R\bar{3}m$), a limited range of solid solubility is expected to occur. Earlier, Belik et al. reported that the strontium solubility in $Ca_{3-x}Sr_x(PO_4)_2$ is as high as x = 2.31 at 1000 °C[35] or $x \approx 2.40$.[36] Thus, in the present study, to get rid of possible impurities, the Sr substitution in $Ca_{3-x}Sr_x(PO_4)_2$:Eu^{2+} is designed to be restricted over the $0 \le x \le 2$ range.

To begin with, the XRD refinements were conducted to confirm the phase purity of the $Ca_{3-x}Sr_x(PO_4)_2$:Eu^{2+} ($0 \le x \le 2$) samples prepared by a similar technology. The previous refinement results for the samples with x = 0 ($Ca_3(PO_4)_2$), x = 1.00 ($Ca_2Sr(PO_4)_2$), and x = 2.00 ($CaSr_2(PO_4)_2$) proved the pure phase feature. The refinements suggest that $Ca_{3-x}Sr_x(PO_4)_2$ exhibits a pure phase formation in the $0 \le x \le 2$ range, and the compounds are isomorphic with the whitlockite, space group $R3c$. Herein, the XRD patterns of three supplemental samples with x = 0.10 ($Ca_{2.9}Sr_{0.1}(PO_4)_2$), x = 0.30 ($Ca_{2.7}Sr_{0.3}(PO_4)_2$), and x = 0.50 ($Ca_{2.5}Sr_{0.5}(PO_4)_2$) were collected and also performed with Rietveld refinements. The observed (black), calculated (red), and difference (gray) XRD profiles for the refinements are shown in Figure 1, and the main parameters of the processing are provided in Table 1. All peaks of the patterns were successfully indexed by a trigonal cell with parameters close to those of $Ca_3(PO_4)_2$;[19] thus, the structure of $Ca_3(PO_4)_2$ was taken as the starting model for the refinements. The results show that the four sites of Ca1, Ca2, Ca3, and Ca4

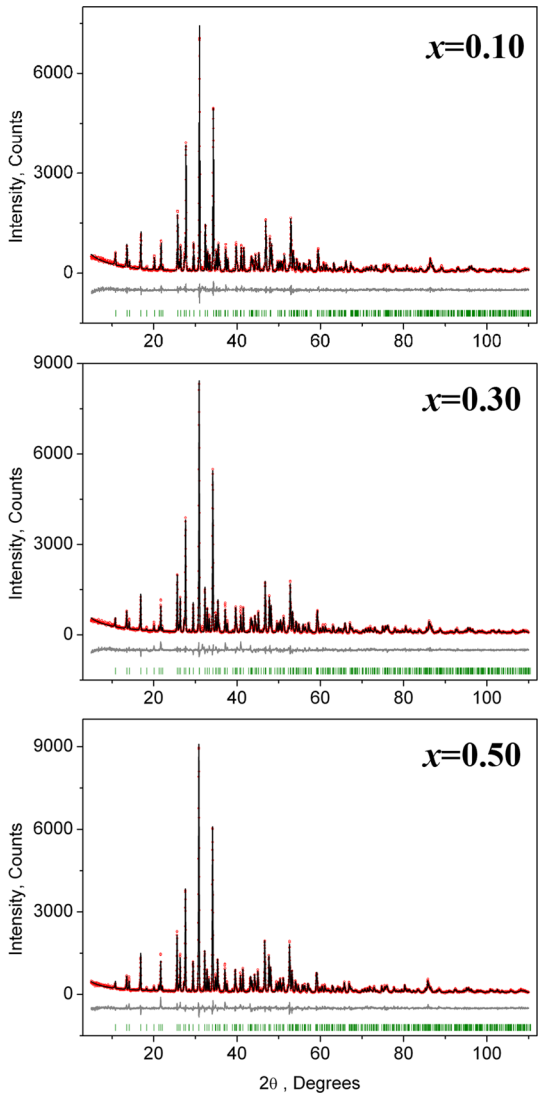

Figure 1. Observed (black), calculated (red), and difference (gray) XRD profiles for the $Ca_{3-x}Sr_x(PO_4)_2$ (x = 0.10, 0.30, 0.50) samples refined by the Rietveld method. Bragg reflections are indicated with green tick marks.

dx.doi.org/10.1021/ic501679f | Inorg. Chem. 2014, 53, 11119−11124

Table 1. Main Parameters of Processing and Refinement of the $Ca_{3-x}Sr_x(PO_4)_2$ (x = 0.10, 0.30, 0.50) Samples

	$Ca_{2.9}Sr_{0.1}(PO_4)_2$	$Ca_{2.7}Sr_{0.3}(PO_4)_2$	$Ca_{2.5}Sr_{0.5}(PO_4)_2$
x	0.1	0.3	0.5
space group	*R3c*	*R3c*	*R3c*
a, Å	10.4482(3)	10.4757(4)	10.5009(4)
c, Å	37.4086(11)	37.4923(15)	37.6282(16)
V, Å^3	3536.6(2)	3563.2(3)	3593.3(3)
2θ interval, deg	5−110	5−110	5−110
no. of rflns	510	513	518
no. of params of refinement	85	85	85
R_{wp}, %	11.84	12.18	11.28
R_p, %	8.58	8.99	8.51
R_{exp}, %	7.01	6.66	6.47
χ^2	1.69	1.83	1.74
R_B, %	2.66	4.08	3.64

ions can be occupied by both Ca and Sr ions with various occupations defined by the chemical composition, and the Ca5 site can only be occupied by Ca ions.[31] The refinements were stable and ended with low R factors (Table 1). Crystallographic information files (CIF) of the three samples $Ca_{3-x}Sr_x(PO_4)_2$ (x = 0.1, 0.3, 0.5) are given in the Supporting Information. Furthermore, a practically linear increase of the cell volume V per increase in x (shown in Figure S1 in the Supporting Information) proves that the Sr ions are incorporated in the compounds according to the nominal chemical formula.

On the basis of the phase purity confirmation, the photoluminescence emission (PL) evolution of the $Ca_{3-x}Sr_x(PO_4)_2:Eu^{2+}$ ($0 \le x \le 2$) phosphors in response to the cation substitution was further characterized. The normalized PL spectra obtained under the 365 nm UV light excitation are shown in Figure 2. $Ca_3(PO_4)_2:Eu^{2+}$ emits blue light with a relatively symmetric narrow band centered at 416 nm, which is consistent with the literature.[37] However, at the specific substitution level of Ca by Sr, for example, the $Ca_{2.7}Sr_{0.3}(PO_4)_2:Eu^{2+}$ phosphor emits green light instead of blue. Furthermore, the samples with the Sr content of $x > 0.75$ exhibit a broad asymmetric band emission, and the dramatic red shift of the second new emission peak wavelength from 493 to 532 nm was also observed with the continuous introduction of Sr^{2+} into the crystal lattice, as shown in Figure 2. As discussed above, with the increase in x from 0 to 2.00, the composition moves closer to the phase transition point where the space group will change, and the x = 2.00 sample ($CaSr_2(PO_4)_2:Eu^{2+}$) exhibits the most strongly red shifted luminescence. The digital images of selected phosphors under 365 nm UV lamp illumination are also shown in Figure 2, and the corresponding visible light emission (blue → green → greenish white → yellow) variation can be clearly observed with increasing x. Also, the fwhm (full width at half-maximum) values of PL spectra increase with the increase in Sr^{2+} substitution content, reaching 130 nm in $CaSr_2(PO_4)_2:Eu^{2+}$.

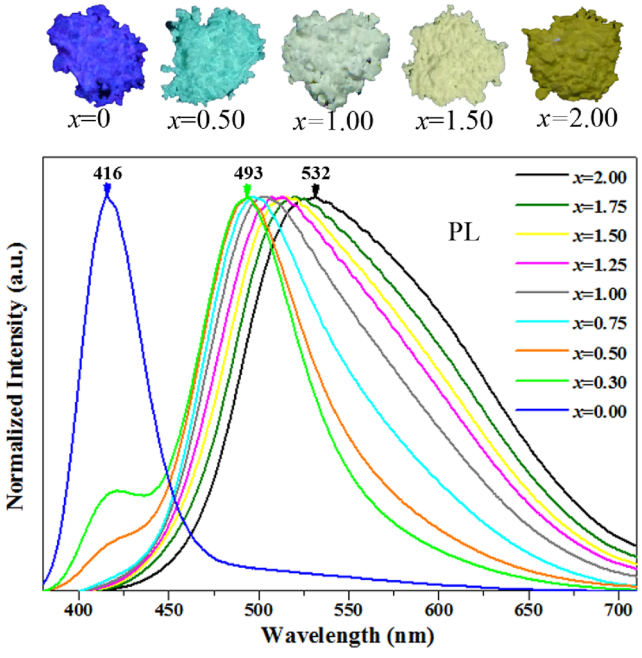

Figure 2. Normalized photoluminescence emission spectra of $Ca_{3-x}Sr_x(PO_4)_2:Eu^{2+}$ (x = 0−2.00) phosphors under 365 nm UV light excitation. The digital images of the selected compositions under the 365 nm UV lamp are also given.

As mentioned above, the primitive part of the $Ca_3(PO_4)_2$ unit cell has five Ca sites which could contain the Ca ions, but the Sr/Eu ions could be only located in four of these sites, and one Ca site is too small to be occupied by Sr/Eu ions.[31] The replacement of Ca by Sr in all these compounds does not change the space group, with the crystal structure remaining the same: i.e., the overall coordination situations of Eu^{2+} in the solutions are the same. Moreover, concerning the local environment of Eu^{2+} ions in the $Ca_{3-x}Sr_x(PO_4)_2:Eu^{2+}$ crystals, the four possible Eu^{2+}-containing sites have different coordination environments. The coordination situation in the first three nearest coordination spheres around the Eu^{2+} sites is shown in Figure 3. As can be seen, the first, second, and third coordination spheres of Eu^{2+} ions consist of O atoms, PO_4 tetrahedrons, and Ca/Sr ions, respectively. At these four sites, different forms of EuO_n polyhedrons and different numbers of

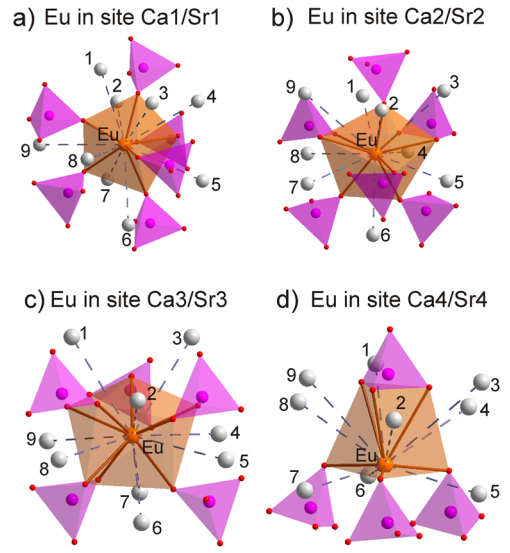

Figure 3. First three nearest coordination spheres of Eu ions which are determined to be located in the four Ca/Sr sites in the unit cell of $Ca_{3-x}Sr_x(PO_4)_2$ ($0 \le x \le 2.00$). The first, second, and third coordination spheres of Eu^{2+} consist of O atoms, PO_4 tetrahedrons, and Ca/Sr ions, respectively. Each Eu site has nine coordinating Ca/Sr ions, which are marked by numbers.

dx.doi.org/10.1021/ic501679f | *Inorg. Chem.* 2014, 53, 11119−11124

coordinating PO_4 tetrahedrons but the same number of neighboring Ca/Sr ions are observed.

It is very interesting to see that bimodal PL emission occurs in the solid solution phosphors, peaking in the blue and green regions, as shown in Figure 2. A more detailed description of the bimodal emission in the 0−0.75 range with a smaller x interval of 0.10 is shown in Figure 4. The samples with $0.10 \leq x \leq 0.50$ emit in two bands peaking at 416 and 493 nm, whereas the $x = 0$ and $x \geq 0.75$ samples exhibit almost a single band peaking either at 416 nm or at 493 nm. The relative intensities of the two emission bands gradually change in response to the gradual x variation: the green emission is continuously enhanced while the blue emission is inhibited at higher Sr^{2+} content, resulting in tunable PL properties. The photoluminescence excitation spectra of the $Ca_{2.7}Sr_{0.3}(PO_4)_2:Eu^{2+}$ ($x = 0.30$) phosphor (in Figure S2, Supporting Information) monitored at λ_{em} 416 and 493 nm are different, suggesting that the two emission bands originate from different emission centers.

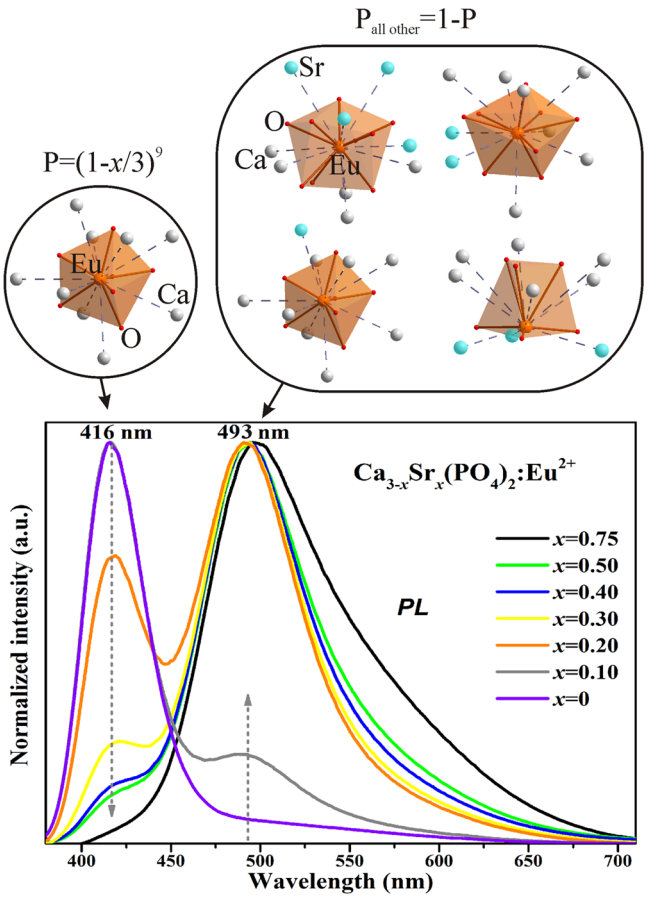

Figure 4. Normalized photoluminescence emission spectra of $Ca_{3-x}Sr_x(PO_4)_2:Eu^{2+}$ ($x = 0$−0.75) under 365 nm UV light excitation. The samples with $0 < x < 0.75$ emit double bands peaking at 416 and 493 nm, respectively. The bands in the blue and green-yellow regions occur due to emission of pure $[EuO_n]$−Ca_9 and $[EuO_n]$−$Ca_{9-y}Sr_y$ blocks, respectively. An increase in Sr concentration results in a decrease in the existence probability of P $[EuO_n]$−Ca_9 blocks and an increase in the existence probability $1 - P$ of $[EuO_n]$−$Ca_{9-y}Sr_y$ blocks, which is correlated with the decreasing intensity of the 416 nm peak and increasing intensity of the 493 nm peak. Also, numerous different $[EuO_n]$−$Ca_{9-y}Sr_y$ blocks originating from random occupation of Ca sites by Sr lead to broadening of the emission band in the green-yellow region.

In the $Ca_3(PO_4)_2:Eu^{2+}$ structure, the Eu ions are coordinated by nine nearby Ca ions in the third coordination sphere and form only the EuO_n−Ca_9 blocks, which are observed to emit blue light under UV excitation, as shown in Figure 3. On doping with Sr, in addition to the EuO_n−Ca_9 blocks, EuO_n−$Ca_{9-y}Sr_y$ (y = 1, 2, ..., 9) blocks appeared. The incorporation of larger Sr^{2+} ions into the structure induces an internal pressure on the lattice and a distortion of the inner EuO_n polyhedrons. Respectively, due to the distortion of EuO_n polyhedrons, the peak wavelength of the band emitted by the EuO_n−$Ca_{9-y}Sr_y$ blocks should be different in reference to the 416 nm peak position related to the EuO_n−Ca_9 blocks (Figure 4). Then, the random distribution of doped Sr^{2+} ions leads to numerous combinations of the EuO_n−$Ca_{9-y}Sr_y$ emitting blocks with different y values and different emission peaks, which ultimately gives a broad integrated emission band peaking in the 493−532 nm region (Figure 4). Generally, the introduction of larger Sr^{2+} ions which compresses the EuO_n polyhedrons should result in a red shift of the peak wavelength. As seen from Figure 3, the introduction of Sr into these crystals is assumed to be most likely to change the third coordination sphere (EuO_n−Ca/Sr interactions), which will then influence the first coordination sphere of Eu^{2+} (EuO_n polyhedron). A detailed evaluation of the distortion of the EuO_n polyhedrons at each site needs accurate synchrotron or neutron experimental data to determine the Ca/Sr/Eu−O bond lengths. From the laboratory X-ray data measured in the present study, it is hard to determine the distortion quantitatively. Therefore, it is difficult to give an explanation as to why the PL peak jumps particularly from 416 to 493 nm.

An assumption from this model is that the intensity of the emission band peaking at 416 nm should be proportional to the number of EuO_n−Ca_9 blocks in the $Ca_{3-x}Sr_x(PO_4)_2$ solid solutions. In addition, this number should decrease with increasing x. The probability that some Ca/Sr sites are occupied only by the Ca ions is equal to $P_0 = (3 - x)/3 = (1 - x/3)$, and thus, the probability that all the nine sites will be occupied by Ca ions is equal to $P = P_0^9 = (1 - x/3)^9$. Therefore, the number N of the EuO_n−Ca_9 blocks normalized to the overall number of blocks N_{all} in the samples is equal to the occurrence probability P of the EuO_n−Ca_9 block: $N/N_{all} = P = (1 - x/3)^9$. Thus, the occurrence probability of all other blocks is equal to $P_{all\ other} = 1 - P = 1 - (1 - x/3)^9$. From another point of view, the normalized intensity of the band peaking at 416 nm should also be equal to N/N_{all}; we then can conclude that $I = (1 - x/3)^9$. This possible dependence is plotted in Figure 5, where the observed change of the normalized intensity of the emission band peaking at 416 nm is found to be well fitted by the function $I(x) = (1 - x/3)^9$, which confirms our hypothesis mentioned above.

The effective color coordinate tuning in response to x variation in the $Ca_{3-x}Sr_x(PO_4)_2:Eu^{2+}$ ($0 \leq x \leq 2.00$) phosphors under λ_{ex} 365 nm in the CIE chromaticity diagram is illustrated in Figure 6. The Sr substitution of Ca in the $Ca_3(PO_4)_2:Eu^{2+}$ crystal lattice leads to the dramatic change of the emission color from blue to green and greenish yellow in the phosphors. Thus, the cation substitution in the whitlockite type compositions is found to be an efficient approach to tune the photoluminescence properties of the $Ca_3(PO_4)_2:Eu^{2+}$ phosphors.

dx.doi.org/10.1021/ic501679f | Inorg. Chem. 2014, 53, 11119−11124

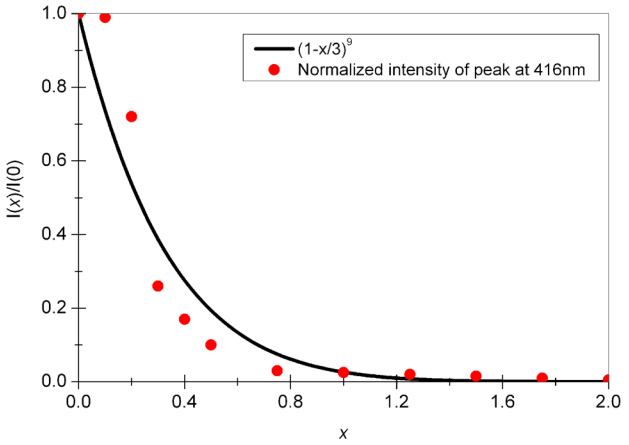

Figure 5. Observed change of the normalized intensity of the 416 nm band fitted by the function $I(x) = (1 - x/3)^9$.

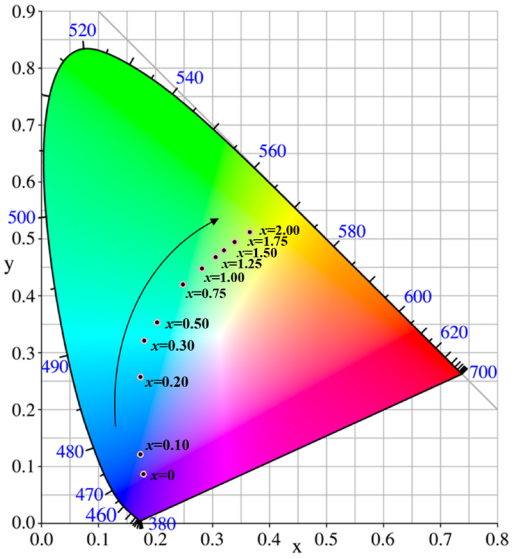

Figure 6. Color coordinates of the $Ca_{3-x}Sr_x(PO_4)_2:Eu^{2+}$ ($0 \leq x \leq 2.00$) phosphors with gradually increasing x in the CIE diagram.

4. CONCLUSIONS

The $Ca_{3-x}Sr_x(PO_4)_2:Eu^{2+}$ solid solution phosphors in the wide range $0 \leq x \leq 2$ have been successfully prepared by a solid-state reaction method. The crystal structure determination by the Rietveld refinement confirms the structural similarity to the mineral whitlockite with space group *R*3*c*. The introduction of Sr changes the third coordination sphere of the Eu^{2+} ions. The unusual double-band photoluminescence emission spectra peaking at 416 and 493 nm originates from the EuO_n-Ca_9 and $EuO_n-Ca_{9-y}Sr_y$ emitting blocks, respectively. The evolution of the number of the two kinds of emitting blocks relates well to the observed intensity evolution of the two emission peaks. In addition, the increased pressure on the EuO_n polyhedron resulting from the doping of larger Sr ions induces the red shift of the second emission band from 493 to 532 nm. Thus, this cation substitution strategy is efficient in tuning the photoluminescence property of the whitlockite type phosphors, especially when the compounds remain isostructural.

■ ASSOCIATED CONTENT

Ⓢ Supporting Information

CIF files giving crystallographic data for $Ca_{3-x}Sr_x(PO_4)_2$ (x = 0.10, 0.30, 0.50) and figures giving the cell volume of $Ca_{3-x}Sr_x(PO_4)_2$:Eu per x and the photoluminescence excitation spectrum of $Ca_{2.7}Sr_{0.3}(PO_4)_2:Eu^{2+}$. This material is available free of charge via the Internet at http://pubs.acs.org.

■ AUTHOR INFORMATION

Corresponding Authors

*E-mail for Z.H.: huang118@cugb.edu.cn.
*E-mail for Z.X.: xiazg@ustb.edu.cn.

Notes

The authors declare no competing financial interest.

■ ACKNOWLEDGMENTS

This work was supported by the National Natural Science Foundations of China (Grant Nos. 51032007, 51002146, 51272242), the Research Fund for the Doctoral Program of Higher Education of China (Grant No. 20130022110006), the Natural Science Foundations of Beijing (2132050), the Program for New Century Excellent Talents in University of Ministry of Education of China (NCET-12-0950), Beijing Nova Program (Z131103000413047), and Beijing Youth Excellent Talent Program (YETP0635). V.V.A. acknowledges the Ministry of Education and Science of the Russian Federation for financial support.

■ REFERENCES

(1) Lin, C. C.; Liu, R. S. *J. Phys. Chem. Lett.* **2011**, *2*, 1268−77.
(2) Xia, Z. G.; Zhang, Y. Y.; Molokeev, M. S.; Atuchin, V. V.; Luo, Y. *Sci. Rep.* **2013**, *3*, 3310−3317.
(3) Wu, W. W.; Xia, Z. G. *RSC Adv.* **2013**, *3*, 6051−6057.
(4) Tang, Y. S.; Hu, S. F.; Lin, C. C.; Bagkar, N. C.; Liu, R. S. *Appl. Phys. Lett.* **2007**, *90*, 151108.
(5) Zhang, S. Y.; Nakai, Y.; Tsuboi, T.; Huang, Y. L.; Seo, H. J. *Inorg. Chem.* **2011**, *50*, 2897−2904.
(6) Huang, C. H.; Liu, W. R.; Chen, T. M. *J. Phys. Chem. C* **2010**, *114*, 18698−18701.
(7) Huang, C. H.; Chen, T. M. *Opt. Express* **2010**, *18*, 5089−5089.
(8) Guo, N.; Huang, Y. J.; You, H. P.; Yang, M.; Song, Y. H.; Liu, K.; Zheng, Y. H. *Inorg. Chem.* **2010**, *49*, 10907−10913.
(9) Huang, C. H.; Chen, T. M.; Liu, W. R.; Chiu, Y. C.; Yeh, Y. T.; Jang, S. M. *ACS Appl. Mater. Interfaces* **2010**, *2*, 259−264.
(10) Guo, N.; Huang, Y. J.; Jia, Y. C.; Lv, W. Z.; Zhao, Q.; Lü, W.; Xia, Z. G.; You, H. P. *Dalton Trans.* **2013**, *42*, 941−947.
(11) Guo, N.; Lü, W.; Jia, Y. C.; Lv, W. Z.; Zhao, Q.; You, H. P. *ChemPhysChem* **2013**, *14*, 192−197.
(12) Guo, N.; Zheng, Y. H.; Jia, Y. C.; Qiao, H.; You, H. P. *J. Phys. Chem. C* **2012**, *116*, 1329−1334.
(13) Guo, N.; Jia, Y. C.; Lü, W.; Lv, W.; Zhao, Q.; Jiao, M.; Shao, B.; You, H. P. *Dalton Trans.* **2013**, *42*, 5649−5654.
(14) Jia, Y. C.; Lü, W.; Guo, N.; Lü, W.; Zhao, Q.; You, H. P. *Phys. Chem. Chem. Phys.* **2013**, *15*, 6057−6052.
(15) Guo, N.; Huang, Y. J.; Yang, M.; Song, Y.; Zheng, Y. H.; You, H. P. *Phys. Chem. Chem. Phys.* **2011**, *13*, 15077−15082.
(16) Liu, W. R.; Huang, C. H.; Yeh, C. W.; Tsai, J. C.; Chiu, Y. C.; Yeh, Y. T.; Liu, R. S. *Inorg. Chem.* **2012**, *51*, 9636−9641.
(17) Liu, W. R.; Chiu, Y. C.; Yeh, Y. T.; Jang, S. M.; Chen, T. M. *J. Electrochem. Soc.* **2009**, *156*, J165−169.
(18) Huang, C. H.; Chen, T. M. *Inorg. Chem.* **2011**, *50*, 5725−5730.
(19) Dickens, B.; Schroeder, L. W.; Brown, W. E. *J. Solid State Chem.* **1974**, *10*, 232−248.
(20) Calvo, C.; Gopal, R. *Am. Mineral.* **1975**, *60*, 120−133.

(21) Zatovsky, I. V.; Strutynska, N. Yu.; Baumer, V. N.; Slobodyanik, N. S.; Ogorodnyk, I. V.; Shishkin, O. V. *J. Solid State Chem.* **2011**, *184*, 705−711.
(22) Strutynska, N. Yu.; Zatovsky, I. V.; Ogorodnyk, I. V.; Slobodyanik, N. S. *Acta Crystallogr., Sect. E* **2013**, *69*, i23.
(23) Zatovsky, I. V.; Strutynska, N. Yu.; Baumer, V. N.; Shishkin, O. V.; Slobodyanik, N. S. *Acta Crystallogr., Sect. E* **2007**, *E63*, i180−181.
(24) Lazoryak, B. I.; Belik, A. A.; Kotov, R. N.; Leonidov, I. A.; Mitberg, E. B.; Karelina, V. V.; Kellerman, D. G.; Stefanovich, S. Yu.; Avetisov, A. K. *Chem. Mater.* **2003**, *15*, 625−631.
(25) Zatovsky, I. V.; Ogorodnyk, I. V.; Strutynska, N. Yu.; Slobodyanik, N. S.; Sharkina, N. O. *Acta Crystallogr., Sect. E* **2010**, *E66*, i41−42.
(26) Belik, A. A.; Izumi, F.; Ikeda, T.; Okui, M.; Malakho, A. P.; Morozov, V. A.; Lazoryak, B. I. *J. Solid State Chem.* **2002**, *168*, 237−244.
(27) Lazoryak, B. I.; Strunenkova, T. V.; Golubev, V. N.; Vovk, E. A.; Ivanov, L. N. *Mater. Res. Bull.* **1996**, *31*, 207−216.
(28) Lazoryak, B. I.; Morozov, V. A.; Belik, A. A.; Stefanovich, S. Yu.; Grebenev, V. V.; Leonidov, I. A.; Mitberg, E. B.; Davydov, S. A.; Lebedev, O. I.; Tendeloo, G. V. *Solid State Sci.* **2004**, *6*, 185−195.
(29) Deyneko, D. V.; Stefanovich, S. Yu.; Mosunov, A. V.; Baryshnikova, O. V.; Lazoryak, B. I. *Inorg. Mater.* **2013**, *49*, 807−812.
(30) Xia, Z. G.; Liu, H. K.; Li, X.; Liu, C. Y. *Dalton Trans.* **2013**, *42*, 16588−16595.
(31) Ji, H. P.; Huang, Z. H.; Xia, Z. G.; Molokeev, M. S.; Atuchin, V. V.; Fang, M. H.; Huang, S. F. *Inorg. Chem.* **2014**, *53*, 5129−35.
(32) *TOPAS V4.2: General profile and structure analysis software for powder diffraction data−User's Manual*; Bruker AXS: Karlsruhe, Germany. 2008.
(33) Matraszek, A. *J. Solid State Chem.* **2013**, *203*, 86−91.
(34) Fix, W.; Heymann, H.; Heinke, R. *J. Am. Ceram. Soc.* **1969**, *52*, 346−347.
(35) Belik, A. A.; Izumi, F.; Stefanovich, S. Yu.; Malakho, A. P.; Lazoryak, B. I.; Leonidov, I. A.; Leonidova, O. N.; Davydov, S. A. *Chem. Mater.* **2002**, *14*, 3197−3105.
(36) Bigi, A.; Foresti, E.; Gandolfi, M.; Gazzano, M.; Roveri, N. *J. Inorg. Biochem.* **1997**, *66*, 259−265.
(37) Lagos, C. C. *J. Electrochem. Soc.* **1970**, *117*, 1189−1193.